

## **Deep Blur Multi-Model (DeepBlurMM) - a strategy to mitigate the impact of unsharp image areas in computational pathology**

Authors

Yujie Xiang<sup>1</sup>, Bojing Liu<sup>1</sup>, Mattias Rantalainen<sup>1,2\*</sup>

<sup>1</sup> *Department of Medical Epidemiology and Biostatistics, Karolinska Institutet, Stockholm, Sweden*

<sup>2</sup> *MedTechLabs, BioClinicum, Karolinska University Hospital, Solna, Stockholm, Sweden*

\* Correspondence to [mattias.rantalainen@ki.se](mailto:mattias.rantalainen@ki.se)

Keywords

computational pathology, image analysis, artificial intelligence, deep learning, quality control

### **Abstract**

AI-based analysis of histopathology whole slide images (WSIs) is central in computational pathology. However, image quality, including unsharp areas of WSIs, impacts model performance. We investigate the impact of blur and propose a multi-model approach to mitigate negative impact of unsharp image areas. In this study, we use a simulation approach, evaluating model performance under varying levels of added Gaussian blur to image tiles from >900 H&E-stained breast cancer WSIs. To reduce impact of blur, we propose a novel multi-model approach (DeepBlurMM) where multiple models trained on data with variable amounts of Gaussian blur are used to predict tiles based on their blur levels. Using histological grade as a principal example, we found that models trained with mildly blurred tiles improved performance over the base model when moderate-high blur was present. DeepBlurMM outperformed the base model in presence of moderate blur across all tiles (AUC:0.764 vs. 0.710), and in presence of a mix of low, moderate, and high blur across tiles (AUC:0.821 vs. 0.789). Unsharp image tiles in WSIs impact prediction performance. DeepBlurMM

improved prediction performance under some conditions and has the potential to increase quality in both research and clinical applications.

## Introduction

Computational pathology<sup>1</sup> leverages artificial intelligence (AI) for the analysis of hematoxylin and eosin (H&E) stained digital histopathology whole slide images (WSIs), and enables model-based solutions both for routine pathology tasks and for precision medicine<sup>2</sup>. Digital WSIs are the core data modality in digital pathology. WSIs are generated by scanning and digitising a high-resolution pathological image of a tissue sample<sup>3</sup>, and can subsequently be used both for manual inspection by a pathologist, or analysed by computer models. Deep convolutional neural networks (CNNs) are central in computational pathology, and have enabled a range of applications from routine pathology tasks, such as cancer detection and grading<sup>2</sup>, to predictive medicine applications, such as prognostic patient stratification<sup>4</sup> and prediction of treatment response<sup>2</sup>.

However, WSI image quality is rarely perfect and uniform, and there is often quality variability across different regions within a WSI, characterised by e.g., discrepancies in sharpness and the presence of areas with varying degrees of blur<sup>5,6</sup>. Image blur, commonly resulting from the scanning processes of WSI<sup>5,7</sup>, can adversely affect the performance of deep learning models in the analysis of WSIs<sup>8-10</sup>. Reduced performance is particularly undesirable in clinical applications that require high accuracy under real-world conditions, and sometimes with less-than-ideal image quality.

Current strategies to mitigate the impact of unsharp areas in WSIs typically involve identifying and excluding blurred regions from the analysis<sup>11-16</sup>. In instances where the blurry area is extensive, an entire WSI may be discarded<sup>11</sup>, while re-scanning or re-preparation of a tissue slide is a possibility, it causes waiting times and additional costs. In the common situation of WSIs with reduced sharpness in some local areas, re-scanning may not help either. Exclusion of whole WSIs, or local areas, when

applying computational models in research or clinical applications, may lead to information loss, bias, incomplete understanding of histopathological features, and reduced prediction performance. Despite previous efforts in identifying low quality images at the WSI level<sup>11</sup> or patch level<sup>17</sup>, to our knowledge, no solutions have been proposed for actively managing various degrees of blur on WSIs at the modelling stage to improve model performance and robustness.

In this study, we first investigate the impact of image sharpness on deep CNN classification performance by simulating multiple levels of blur through the application of various amounts of Gaussian blur to WSIs. Subsequently, we introduce a novel multi-model approach designed to alleviate the impact of image focus on model performance, aiming to offer a robust prediction in the presence of under-focused image regions. Throughout this study, we use the binary classification task of distinguishing between breast cancer Nottingham Histological Grade (NHG)<sup>14,18</sup>, particularly 1 vs. 3, as a principal example to illustrate the methodology. See Figure 1 for an overview.

Real-world data is rarely of perfect quality. By acknowledging this fact and actively exploring the impact of variable image quality as well as strategies to mitigate this issue, we propose solutions to enhance the robustness of computational pathology models. This has the potential to improve prediction performance in both clinical and research contexts.

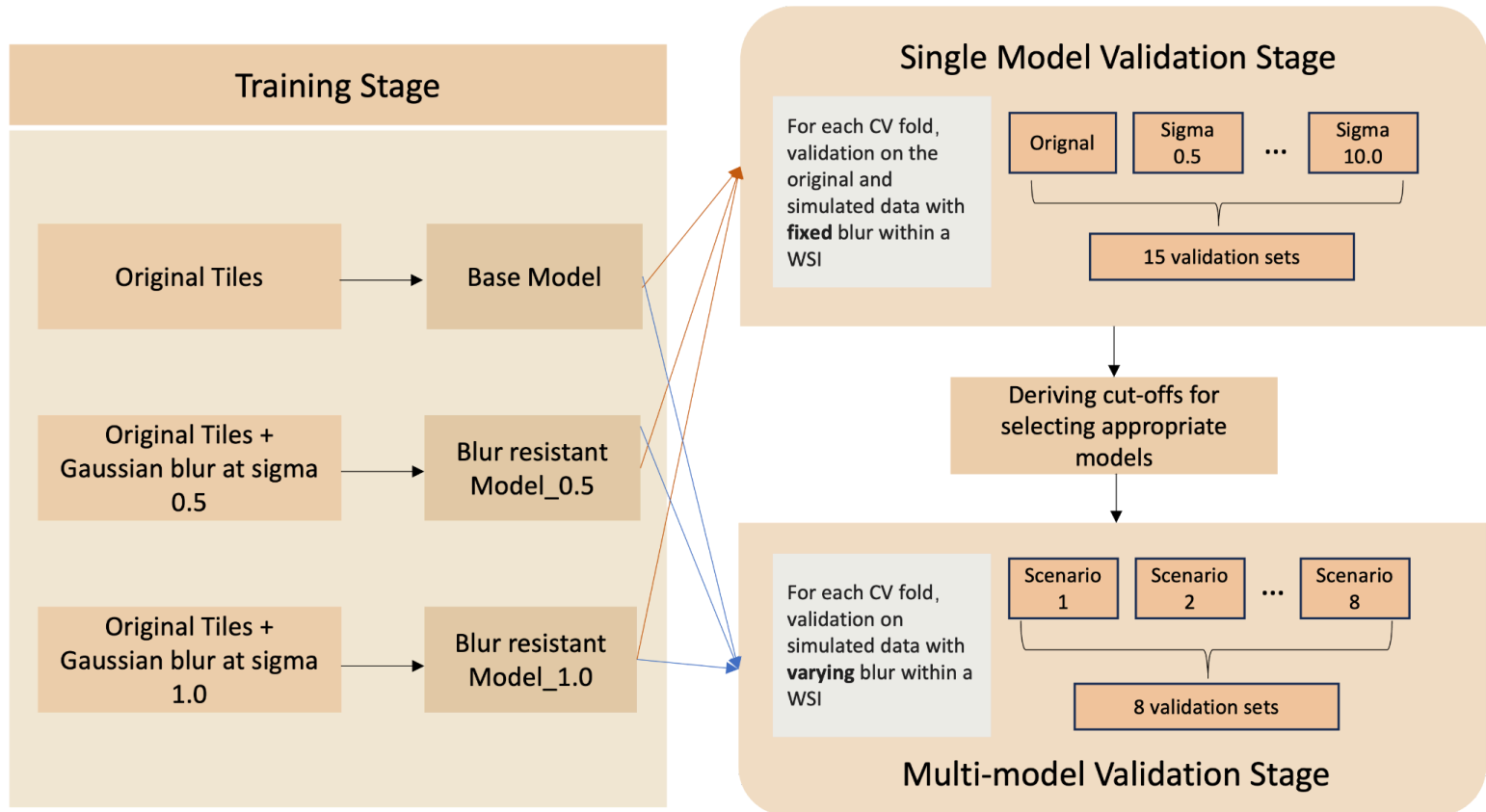


Figure 1. Overview of the study design based on an example task of predicting Nottingham Histological Grade (NHG) 1 vs 3. We trained three models on datasets with varying sharpness: original tiles, and original tiles with simulated Gaussian blur of sigma 0.5 and 1.0. These models were evaluated on an original validation set and 14 additional sets. Each validation set had a constant level of Gaussian blur applied to WSIs, with sigma ranging from 0.5 to 10.0. Based on the models' performance across these sets, we established sigma cut-offs to determine a suitable model for predicting tiles with various levels of blurring. The cut-offs categorised the tiles into sharp or slight blur, moderate blur, and high blur. To emulate real-world scenarios with variable blurring within a WSI, we simulated validation sets with eight different blur scenarios. A multi-model approach (DeepBlurMM) was applied for the prediction. All experiments were performed using a 5-fold CV.

# Materials and Methods

## Dataset

This study was based on data from a Swedish breast cancer cohort of female patients (N=2093). This cohort incorporated patients diagnosed at Stockholm's South General Hospital between 2012 and 2018, for whom archived histological slides and corresponding NHG grade were available<sup>15</sup>. As the study was focused on the classification of NHG 1 vs 3 as an example task, we excluded patients diagnosed with NHG 2 or with missing NHG data from the analysis. The final dataset included 916 patients (363 NHG 1, 553 NHG 3) (with one WSI per patient).

Data were split into 5-fold cross-validation (CV) sets (80% training and 20% validation) at the patient level (Figure 2), with a balanced distribution of NHG 1 and 3 cases across each fold. For model selection and parameter tuning, we further divided each training set at the patient level into 80% for training and 20% for tuning (Supplementary Table S1), stratified by NHG.

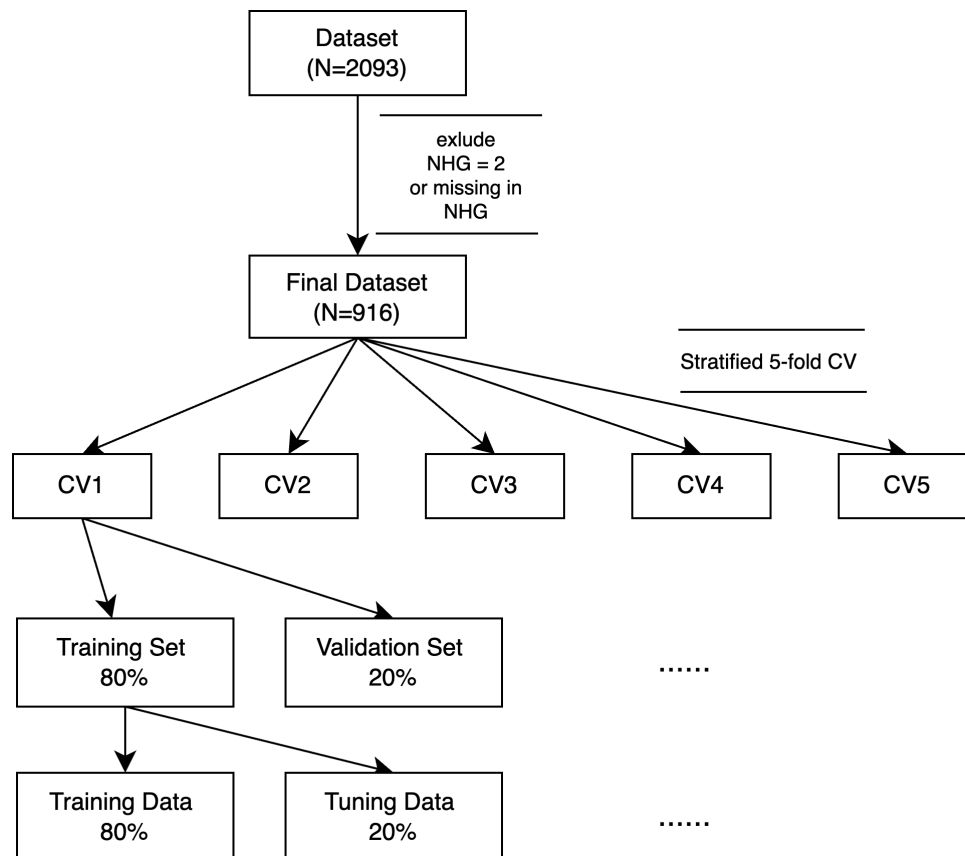


Figure 2. Data split structure

## Image pre-processing

We applied the same pre-processing and quality control steps to H&E stained WSIs, as described previously<sup>14,15</sup>. In brief, the pre-processing steps comprised 1) generating tissue masks using an Otsu threshold of 25 to exclude background regions, 2) tiling WSIs into  $598 \times 598$  pixel image patches at 20X resolution (pixel size =  $271 \times 271 \mu\text{m}$ ), 3) calculating the variance of Laplacian (LV) as a measurement of sharpness for each image tile, and discarding those with LV less than 500, indicating blurry or being out-of-focus, 4) applying a modified stain normalisation method proposed by Macenko et al.<sup>19</sup> across WSIs, and 5) applying a previously trained CNN model to detect cancer regions<sup>14</sup>. These pre-processed tiles were subsequently used in all model optimisation and analysis described below.

## Simulation of Gaussian blur on WSIs for model development

Taking a simulation approach, we employed a Gaussian Blur function, also known as Gaussian Smoothing, to modulate the blurring intensity in the pre-processed tiles<sup>20</sup>. The function operates by averaging neighbouring pixels based on weights from a Gaussian distribution (i.e. Gaussian kernel)<sup>21,22</sup>. In this way, we modulated the blurring intensity of image tiles allowing us to systematically investigate the impact of varying degrees of blur on model performance.

The Gaussian kernel is defined as:

$$\mathbf{G}(x, y) = \frac{1}{2\pi\sigma^2} e^{-\frac{x^2+y^2}{2\sigma^2}} \quad 23$$

where  $x$  and  $y$  represent the spatial position relative to the centre of the kernel, and  $\sigma$  is the standard deviation of the Gaussian distribution, with larger  $\sigma$  resulting in a broader spread of the Gaussian kernel and a greater blur<sup>24</sup>. The kernel size is determined by  $\sigma$  mathematically. The blurring effect is represented mathematically as:

$$I'(x, y) = (I * G)(x, y) \quad 25$$

where  $I'(x, y)$  denotes the blurred image resulting from the convolution of original image  $I$  with Gaussian kernel  $G$ <sup>25,26</sup>.

We hypothesised that a model trained on blurry images might outperform one trained on focused images when predicting on unsharp images. To test this hypothesis, we simulated varying levels of blurriness on WSIs both for model training and performance evaluation (Figure 1). First, we simulated two blurred training sets at  $\sigma = 0.5$  and  $\sigma = 1.0$ . All tiles in the training sets were given a Gaussian blur with  $\sigma = 0.5$  or  $1.0$ , respectively. These two sets of blurred data will be used to train blur-resistant models as described below. To validate the performance of these models on images with varying degrees of blur, we simulated 14 validation sets, each subjected to Gaussian blur at different sigma levels, from subtle to significant: 0.5, 1.0, 1.5, 2.0, 2.5, 3.0, 3.5, 4.0, 5.0, 6.0, 7.0, 8.0, 9.0, and 10.0

(Figure 3). A sigma of zero indicated no added blur (i.e. using the original tile). This served as a baseline that was compared to the effects of various levels of blurring. The original image tile was sharp, with all morphological details clearly visible. On the other hand, with increasing sigma values, blur effects gradually intensified on the image tile. From sigma 0.5 to 1.5, certain morphologies remained visible, but with sigma values of 6.0-10.0, all morphological structures were smoothed out and no longer distinguishable.

## Mapping tiles with the simulated Gaussian blur to Variance of Laplacian (LV)

We were interested in understanding how tiles with simulated Gaussian blur could reflect real-world images with different qualities. As LV serves as a quantitative index of sharpness and has been commonly employed in evaluating the quality of histopathology images<sup>27,28</sup>, we established a mapping between different levels of Gaussian blur (i.e. with sigma ranging from 0.5 to 7.0) and LV (Figure 4). This mapping facilitated our understanding of how the simulated blurry tiles correspond to the LV levels in real-world histopathology images. First, for a representative assessment, we randomly selected 10,000 tiles from the original dataset. Second, we applied different sigma values to the selected original tiles to introduce blur. Last, the LV was computed for each original tile and tile after applying various Gaussian blur. A higher LV indicates a sharper tile.



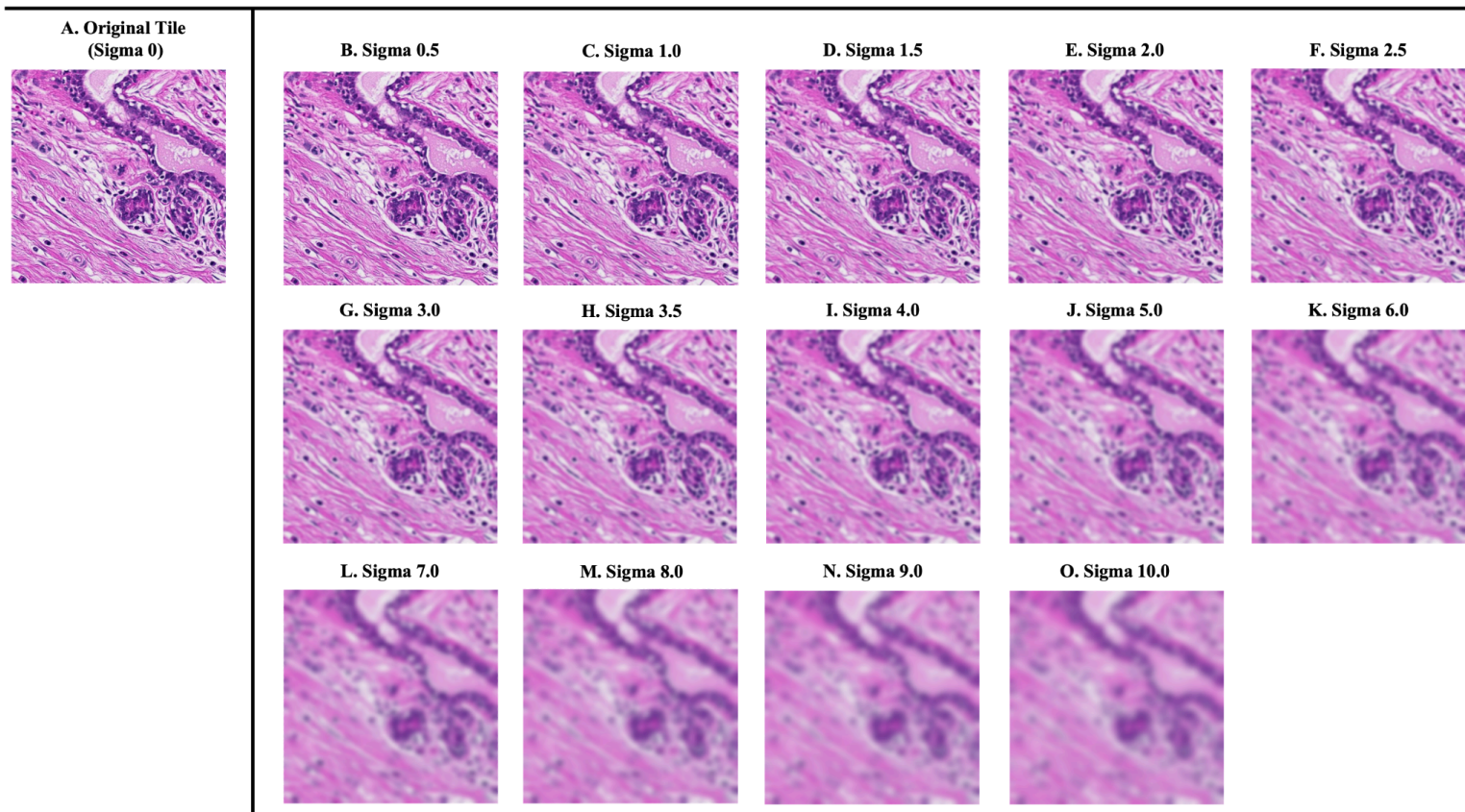


Figure 3. Degree of Gaussian blur in histopathology images. Image (A) represents the original, unblurred image, serving as the baseline for the analysis. Images (B-O) show the application of Gaussian blur with increasing sigma values from 0.5 to 10.0. Specifically, these images illustrate the effect of varying degrees of blurring added to the original histopathology image.

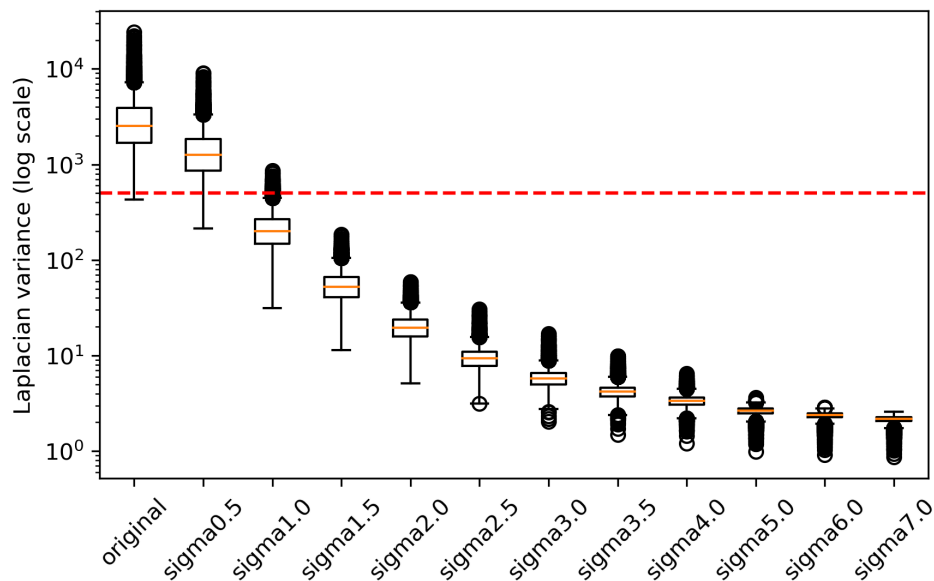


Figure 4. The Laplacian variance for tiles with different Gaussian blur levels. The y-axis shows Laplacian variance values plotted on a logarithmic scale. The red line represents the LV threshold of 500.

## Development of base model and blur-resistant models

The base model was trained with original image tiles (no added Gaussian blur) to classify NHG 1 vs 3 (Figure 1). We chose a commonly used CNN architecture, i.e. ResNet18, initialised with ImageNet weights<sup>29</sup>. The model was optimised using the Stochastic Gradient Descent (SGD)<sup>30</sup> optimiser with a cross-entropy loss function. We used a mini-batch size of 32 per step, and each optimisation partial epoch consisted of 1250 steps (40,000 tiles) for training. We randomly selected 625 mini-batches (20,000 tiles) in the tuning set to evaluate model performance at each epoch end. Early stopping was applied when the loss did not decrease after the patience of 25 partial epochs or continued training for a maximum of 500 epochs. Data augmentation of rotation and flips was applied during model training. The learning rate (LR) was optimised at  $1 \cdot 10^{-5}$ , and we implemented reducing LR by a factor of 0.5 with the patience of 13 partial epochs. The models were trained using PyTorch 1.13.0 and RayTune 2.1.0 frameworks on four RTX 2080 Ti GPUs. The optimised Model\_base was subsequently validated on the original validation set (no added blur) and on the 14 simulated validation sets applied with different Gaussian blur (Figure 1).

Furthermore, we developed two blur-resistant models, Model\_0.5 and Model\_1.0, trained on data with simulated Gaussian blur with  $\sigma$  of 0.5 and 1.0, respectively (Figure 1). The CNN model structure was the same as used in Model\_base. We optimised the LR for Model\_0.5 at 1-e5 and Model\_1.0 at 1-e6, while keeping other hyperparameters consistent with the Model\_base. Similarly, the two blur-resistant models were validated on the original validation set and 14 validation sets applied with Gaussian blur (Figure 1).

We calculated and compared the Area Under the Curve (AUC) for the validation performance of the base model and blur-resistant models across the original and 14 simulated validation sets with Gaussian blur added, at both tile (Figure 5a) and slide level (Figure 5b). The aggregation from tile to slide level was achieved by using the 75 percentile of the tile-level prediction<sup>31</sup>. The training and validation approach was implemented using a 5-fold CV.

## Development of the multi-model prediction approach

The proposed multi-model method, i.e. DeepBlurMM, uses a set of models (trained on original data and data with added Gaussian blur), and predicts each tile through the most optimal model based on the estimated level of blur in each tile. Through the proposed method, we hope to mitigate the impact of variability in image sharpness and consequently enhance the prediction performance.

### *Establishing cut-offs determining suitable models to predict on tiles with different levels of blur*

Consistent with our hypothesis, blur-resistant models appeared to be more robust than the base model when predicting on under-focused images. According to the slide level prediction in Figure 5a, we observed two critical sigma cut-offs: Model\_0.5 outperformed Model\_base on images with Gaussian blur greater than sigma 1.5, and Model\_1.0 outperformed Model\_0.5 on images with Gaussian blur

greater than sigma 6.0. Based on the mapping between Gaussian blur and LV (Figure 5c), we identified cut-offs according to LV as follows: LV of 25 corresponds to images with Gaussian blur of sigma 1.5 approximately, and LV of 2 corresponds to images with Gaussian blur of sigma 6.0 approximately. This indicated that for prediction on natural histopathology images with a focus quality of  $LV > 25$ , Model\_base is preferred. For images with  $2 \leq LV \leq 25$ , Model\_0.5 should be selected, and for images with  $LV < 2$ , Model\_1 should be recommended.

### *Simulating varying Gaussian blur within WSIs in validation sets emulating real-world data*

To validate the multi-model prediction approach mentioned above, we simulated blurred validation sets mimicking the real-world data where WSIs have regions with various focus qualities. Our simulation involved incorporating varying Gaussian blur for different proportions of tiles within a single WSI. This simulation was performed under eight scenarios (Table 1). For the simulation purpose, we defined three Gaussian blur groups based on the observed sigma cut-offs of 1.5 and 6.0, i.e. Group A:  $\sigma \sim U(0, 1.5)$  representing slight blur, Group B:  $\sigma \sim U(1.5, 6.0)$  representing moderate blur, and Group C:  $\sigma \sim U(6.0, 10.0)$  representing heavy blur. For each sigma group, the application of Gaussian blur on a single tile was determined by random sampling from a uniform distribution<sup>32</sup> defined by the corresponding sigma range. This approach ensured that the degree of blur applied to the tiles was both randomised and evenly distributed within predefined ranges. These simulated blurring validation sets were used to evaluate the performance of different model approaches in the subsequent steps.

### *Validation of the multi-model prediction approach*

We validated the DeepBlurMM prediction performance based on simulated data with varying blur regions within the WSIs mentioned above. In order to mimic the real-world scenario where the image focus quality was commonly measured by LV, we calculated the LV for the simulated tiles, and assigned an appropriate model for prediction based on the LV cut-offs of 25 and 2. The DeepBlurMM

validation performance was evaluated using the 5-fold CV on both tile and slide levels, and compared to the performance of the base model. Details in Gaussian simulation and model validation are shown in Table 2.

Table 1. Overview of the eight simulation scenarios\*

| Scenarios | Group A % | Group B % | Group C % |
|-----------|-----------|-----------|-----------|
| 1         | 100       | 0         | 0         |
| 2         | 0         | 100       | 0         |
| 3         | 0         | 0         | 100       |
| 4         | 50        | 25        | 25        |
| 5         | 25        | 50        | 25        |
| 6         | 25        | 25        | 50        |
| 7         | 50        | 50        | 0         |
| 8         | 80        | 15        | 5         |

\*Eight simulation scenarios assigned varying proportions of tiles within a WSI to Gaussian blur A, B, and C groups. These simulated datasets were used to validate DeepBlurMM model performance.

Table 2. Algorithm overview - DeepBlurMM

| For each tile within a WSI in each scenario: |  |
|--|--|
| Step 1.                                      | The initial blur level of a tile was denoted by $g$  |
| Step 2.                                      | Each tile within a WSI was randomly assigned into one of the three predefined Gaussian blur groups (Groups A, B, and C) according to a specific scenario listed in Table 1   |
| Step 3.                                      | Apply blur $g_i$ to each tile based on the Gaussian group assignment using a uniform distribution, i.e. $g_i \sim U(a, b)$ with $a$ and $b$ being the range of sigma values for the uniform distribution for the group, and calculate a new blur level $\hat{g} = g + g_i$ |
| Step 4.                                      | Calculate the LV of a blurred tile as:<br>$\theta = LV(\hat{g}) = Var(L * I_{\hat{g}})$ , where $L$ is the Laplacian operator, $I_{\hat{g}}$ is the simulated image with Gaussian blur $\hat{g}$ , and $\theta$ is the estimated LV value for the blurred tile             |
| Step 5.                                      | Assign one suitable model (i.e Model_base, Model_0.5, or Model_1.0) to predict the blurred tile based on the estimated $\theta$ (if $\theta > 25$ , Model_base is assigned; if $2 \leq \theta \leq 25$ , Model_0.5 is assigned; if $\theta < 2$ , Model_1.0 is assigned)   |
| Step 6.                                      | Repeat Steps 2 to 5 until predictions for all tiles in one WSI are generated.  |

## Results

### Impact of simulated blur on deep CNN model performance

We evaluated the prediction performance of the three models on the validation set with original tiles (i.e. no Gaussian blur applied). The AUCs were as follows: 0.888 for Model\_base, 0.878 for Model\_0.5, and 0.778 for Model\_1.0, indicating the superior performance of the baseline model on original images.

Thereafter, we evaluated the performance of the three models on validation sets subject to varying amounts of Gaussian blur (Figure 5a, Figure 5b, and Supplementary Table S2). We noted that all models' performance, at both tile and slide levels, decreased when the intensity of Gaussian blur was

increased (Figures 5a and 5b). At slide level (Figure 5a), Model\_base demonstrated superior performance to the other models under mildly blurred conditions ( $\sigma < 1.5$ ). For images with moderate Gaussian blur ( $1.5 \leq \sigma < 6.0$ ), Model\_0.5 consistently outperformed Model\_base and Model\_1.0. The performance of Model\_1.0 exceeded those of the other two models with extreme blur ( $\sigma \geq 6.0$ ), despite slightly better than random guessing performance. With a  $\sigma > 8.0$ , classification performance deteriorated to a null result (AUC around 0) for all models. The trend for the tile-level performance (Figure 5b) was similar to the slide level performance, although the differences among the three models were much smaller.

According to these findings, the sharpness levels were divided into three groups based on the performance of models: 1) *sharp or slight blur, Group A ( $\sigma$  0 to 1.5)*; 2) *moderate blur, Group B ( $\sigma$  1.5 to 6.0)*; 3) *high blur, Group C ( $\sigma$  larger than 6.0)*. Next, we further investigated the quantifiable relationship between Gaussian blur intensity ( $\sigma$ ) and image sharpness, as measured by LV. Through the analytical plotting (Figure 5c), we discerned the LV thresholds for Gaussian blur groups, which laid a foundation for the implementation of the multi-model approach. The threshold 1 of LV with 500 was the original cut-off used to filter out focused images during pre-processing, which served as boundary-demarcating images of high sharpness. If the blur level of images for prediction is above threshold 2 (LV=25), the Base model should be selected (Group A); if it is between thresholds 2 (LV=25) and 3 (LV=2), Model\_0.5 should be selected (Group B); if it is below thresholds 3 (LV=2), model\_1.0 should be selected (Group C).

## Comparison of performances for DeepBlurMM and the base model

We simulated validation data across eight different scenarios to mimic the real-world data of varying quality. We compared the model performance from the DeepBlurMM and the base model approach (Table 3). DeepBlurMM performed consistently better than the Model\_base. For slide-level prediction performance, in scenarios 8 and 1, where 85% to 100% of the tiles within a WSI were focused or slightly blurred, the performances of the DeepBlurMM and Model\_base were very similar, at both tile

and slide levels. The biggest performance improvement of 7.61% was observed in scenario 2, where all the tiles within a WSI were moderately blurred. From scenarios 4 to 7, where varying proportions of blur were present at all levels, the DeepBlurMM outperformed the Model\_base by 0.35% to 4.94%. In scenario 3, where all tiles were in Group C (most blur), neither of the models provided predictions better than random chance. A similar trend was observed for tile-level predictions.

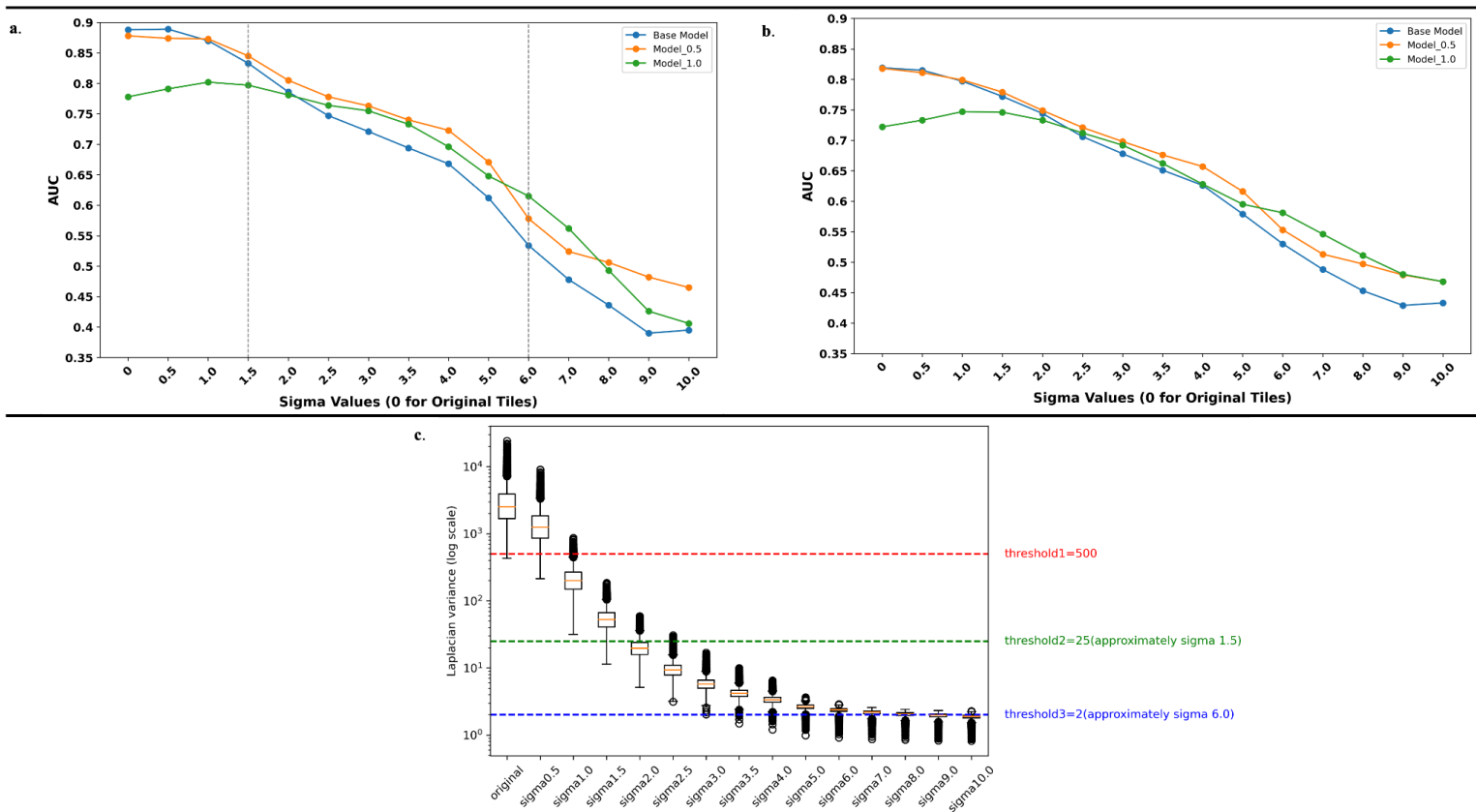


Figure 5. Performance of three models and cut-off points selections. Figure 5a, AUC scores for 3 models at slide level. Based on the AUC comparison among three models, the cut-off points for the three groups are sigma 1.5 and sigma 6.0; Figure 5b, AUC scores for 3 models at tile level; Figure 5c, Specify the variance of Laplacian based on 10,000 tiles with different sigma values. The threshold 1 (LV=500) denoted the original cut-off used to filter out sharp images during preprocessing. Thresholds 2 (LV=25) and 3 (LV=2), corresponding to critical sigmas of 1.5 and 6.0 shown in Figure 5a, were used to select the appropriate model to predict images with varying degrees of blurriness.



Table 3. AUC scores comparison in different scenarios

| Scenarios | % of tiles within a WSI from Gaussian blur group A/B/C | Multi-model (DeepBlurMM) |                    | Model_base        |                    |
|-----------|--|--------------------------|--------------------|-------------------|--------------------|
|           |  | AUC at tile level        | AUC at slide level | AUC at tile level | AUC at slide level |
| 1         | A = 100  | 0.796                    | 0.882              | 0.795             | 0.882              |
| 2         | B = 100  | 0.666                    | 0.764              | 0.641             | 0.710              |
| 3         | C = 100  | 0.532                    | 0.506              | 0.467             | 0.435              |
| 4         | A/B/C = 50/25/25                                       | 0.712                    | 0.861              | 0.696             | 0.858              |
| 5         | A/B/C = 25/50/25                                       | 0.676                    | 0.821              | 0.651             | 0.789              |
| 6         | A/B/C = 25/25/50                                       | 0.646                    | 0.790              | 0.616             | 0.775              |
| 7         | A/B/C = 50/50/0  | 0.735                    | 0.862              | 0.721             | 0.854              |
| 8         | A/B/C = 85/15/5  | 0.769                    | 0.880              | 0.763             | 0.878              |

## Discussion

In this study, we assessed the impact of image blur on the performance of deep learning models for breast cancer grade prediction and proposed a multi-model approach, i.e. DeepBlurMM, to reduce the impact of local unsharpness in WSIs. We found that unsharp images had a measurable impact on model performance, underscoring the importance of data collection and quality control of digital pathology images. Furthermore, our study demonstrated the feasibility of developing models designed to actively handle WSIs with varying degrees of blur locally.

In WSIs, it is not uncommon for some areas of the image to be less sharp than the rest. We took a simulation approach to study the effect of such variable blurring in WSIs. Based on the first set of our results, indicating that deep CNN models can indeed be trained in such a way that they offer better performance compared to a base model (trained on high quality data only), we propose a multi-model approach. Conceptually, this idea is simple, we establish multiple models that offer optimal performance on different blur levels. At inference time, we quantify blurriness at each time, and then use the most suitable of the set of models. Our results showed that under scenarios where there was a mix of slight blur, moderate blur, and high blur, the proposed multi-model approach

(DeepBlurMM) demonstrated better performance than the base model. Taking this approach, the overall prediction performance across different sharpness levels of image quality could be optimised.

During the analysis, we found that the application of Gaussian blur with varying degrees led to a consistent reduction in model performance, measured by AUC at both tile and slide levels. Notably, this decline was more severe at higher blurring levels. The decrease in performance could be related to the fact that the Gaussian blur tended to smooth the tile and reduce high-frequency features relevant to the prediction task at hand. We expect that blurriness will always negatively impact deep learning models in the area of computational pathology. However, depending on the problem, the magnitude of impact might vary. This finding highlights the necessity of quality control in the digital pathology workflow to mitigate the adverse effects of image quality variability. Generally, excluding regions of images with poor quality is a common approach, although it is at the risk of missing important information. However, we also noted that the impact of blur is not drastic, at least not under slight blur or with a minor proportion of the WSI tiles having moderate levels of blur. This suggests that the performance decline might often be minor and may not be a source of major risks in clinical applications, however, this is likely to be very context dependent. At the same time, model performance is likely to be improved by better modelling and quality control steps.

Previous studies have characterised how image quality affects CNN models<sup>10,33</sup>, and proposed assessment tools for detecting the out-of-focus (OOF) regions in WSIs to mitigate its impacts<sup>5,7,11,13</sup>. For example, Kohlberger et al. developed ConvFocus<sup>6</sup> and Senaras et al. developed DeepFocus<sup>34</sup> to exhaustively localise and quantify the severity of OOF regions on WSIs. Rodrigues et al. generated an AI-based tool SlideQC<sup>35</sup> and Janowczyk et al. developed an open-source tool HistoQC<sup>36</sup> for automated quality control of WSIs. The blur tiles or highly blurred entire WSI detected by such approaches will be discarded. Compared to these methods, we used a simple and very fast way to estimate blurriness (i.e. using LV), and there might be an opportunity to achieve even better blur quantification by using more sophisticated methods. However, that would come at the expense of

higher computational time, which is not desirable in large studies with 10,000s of WSIs to be processed. Furthermore, our novel multi-model approach does not need to exclude blurred regions or discard the entire WSI, and we believe the proposed methodology not only preserves valuable pathological information but also improves diagnostic accuracy in digital pathology.

This study has some limitations, including the simulation study that for practical reasons only could cover a specified subset of scenarios. Follow-up studies are needed to investigate the impact of blur on different model architectures and perhaps under other applications. The strengths of this study are that it includes a relatively large number of WSIs, and that the simulation-based approach provides a well-controlled context for both studying the impact of blur and evaluating the performance benefits of novel approaches.

In conclusion, unsharp tiles can reduce the performance of deep learning models in the context of digital and computational pathology. The negative impact of blur is measurable and detectable, but only becomes significant in more extreme situations. This study highlights the value of collecting good-quality image data, the importance of quality control steps and the potential for improved modelling to mitigate some of the problems. The proposed multi-model approach improved performance under some conditions in our simulation study, and the approach might contribute to improving quality in the research context as well as in clinical settings.

## References

1. Bera, K., Schalper, K. A., Rimm, D. L., Velcheti, V. & Madabhushi, A. Artificial intelligence in digital pathology - new tools for diagnosis and precision oncology. *Nat. Rev. Clin. Oncol.* **16**, 703–715 (2019).
2. Acs, B., Rantalainen, M. & Hartman, J. Artificial intelligence as the next step towards precision pathology. *J. Intern. Med.* **288**, 62–81 (2020).
3. Ghaznavi, F., Evans, A., Madabhushi, A. & Feldman, M. Digital imaging in pathology: whole-slide imaging and beyond. *Annu. Rev. Pathol.* **8**, 331–359 (2013).
4. Jaroensri, R. *et al.* Deep learning models for histologic grading of breast cancer and association with disease prognosis. *NPJ Breast Cancer* **8**, 113 (2022).
5. Chen, Y. *et al.* Assessment of a computerized quantitative quality control tool for whole slide images of kidney biopsies. *J. Pathol.* **253**, 268–278 (2021).
6. Kohlberger, T. *et al.* Whole-Slide Image Focus Quality: Automatic Assessment and Impact on AI Cancer Detection. *J. Pathol. Inform.* **10**, 39 (2019).
7. Miranda Ruiz, F. *et al.* CNN stability training improves robustness to scanner and IHC-based image variability for epithelium segmentation in cervical histology. *Front. Med.* **10**, 1173616 (2023).
8. Liu, Y. *et al.* Artificial Intelligence–Based Breast Cancer Nodal Metastasis Detection: Insights Into the Black Box for Pathologists. *Arch. Pathol. Lab. Med.* **143**, 859–868 (2018).
9. Li, Q. *et al.* Rapid Whole Slide Imaging via Dual-Shot Deep Autofocusing. *IEEE Transactions on Computational Imaging* **7**, 124–136 (2021).
10. Dodge, S. & Karam, L. Understanding how image quality affects deep neural networks. in *2016 Eighth International Conference on Quality of Multimedia Experience (QoMEX)* 1–6 (IEEE, 2016).
11. Haghghat, M. *et al.* Automated quality assessment of large digitised histology cohorts by artificial intelligence. *Sci. Rep.* **12**, 5002 (2022).

12. Hang Wu *et al.* Detection of blur artifacts in histopathological whole-slide images of endomyocardial biopsies. *Conf. Proc. IEEE Eng. Med. Biol. Soc.* **2015**, 727–730 (2015).
13. Hossain, M. S. *et al.* Tissue Artifact Segmentation and Severity Assessment for Automatic Analysis Using WSI. *IEEE Access* **11**, 21977–21991 (2023).
14. Wang, Y. *et al.* Improved breast cancer histological grading using deep learning. *Ann. Oncol.* **33**, 89–98 (2022).
15. Sharma, A. *et al.* Development and prognostic validation of a three-level NHG-like deep learning-based model for histological grading of breast cancer. *Breast Cancer Res.* **26**, 17 (2024).
16. Wang, Y. *et al.* Predicting Molecular Phenotypes from Histopathology Images: A Transcriptome-Wide Expression–Morphology Analysis in Breast Cancer. *Cancer Res.* **81**, 5115–5126 (2021).
17. Hosseini, M. S. *et al.* Focus Quality Assessment of High-Throughput Whole Slide Imaging in Digital Pathology. *IEEE Trans. Med. Imaging* **39**, 62–74 (2020).
18. Shawi, R. E., Kilanava, K. & Sakr, S. An interpretable semi-supervised framework for patch-based classification of breast cancer. *Sci. Rep.* **12**, 16734 (2022).
19. Macenko, M. *et al.* A method for normalizing histology slides for quantitative analysis. in *2009 IEEE International Symposium on Biomedical Imaging: From Nano to Macro* 1107–1110 (IEEE, 2009).
20. OpenCV. OpenCV: Smoothing Images. *OpenCV*  
[https://docs.opencv.org/3.4/dc/dd3/tutorial\\_gaussian\\_median\\_blur\\_bilateral\\_filter.html](https://docs.opencv.org/3.4/dc/dd3/tutorial_gaussian_median_blur_bilateral_filter.html).
21. Liu, Y.-Q., Du, X., Shen, H.-L. & Chen, S.-J. Estimating Generalized Gaussian Blur Kernels for Out-of-Focus Image Deblurring. *IEEE Trans. Circuits Syst. Video Technol.* **31**, 829–843 (2021).
22. Hummel, R. A., Kimia, B. & Zucker, S. W. Deblurring Gaussian blur. *Computer Vision, Graphics, and Image Processing* **38**, 66–80 (1987).
23. Lefkimmiatis, S., Bourquard, A. & Unser, M. Hessian-based norm regularization for image restoration with biomedical applications. *IEEE Trans. Image Process.* **21**, 983–995 (2012).
24. OpenCV. Image Filtering. *OpenCV*

[https://docs.opencv.org/4.x/d4/d86/group\\_\\_imgproc\\_\\_filter.html](https://docs.opencv.org/4.x/d4/d86/group__imgproc__filter.html).

25. Flusser, J. *et al.* Recognition of Images Degraded by Gaussian Blur. *IEEE Trans. Image Process.* **25**, 790–806 (2016).
26. Kostková, J., Flusser, J., Lébl, M. & Pedone, M. Image Invariants to Anisotropic Gaussian Blur. in *Image Analysis* 140–151 (Springer International Publishing, 2019).
27. Bansal, R., Raj, G. & Choudhury, T. Blur image detection using Laplacian operator and Open-CV. in *2016 International Conference System Modeling & Advancement in Research Trends (SMART)* 63–67 (ieeexplore.ieee.org, 2016).
28. Pech-Pacheco, J. L., Cristobal, G., Chamorro-Martinez, J. & Fernandez-Valdivia, J. Diatom autofocusing in brightfield microscopy: a comparative study. in *Proceedings 15th International Conference on Pattern Recognition. ICPR-2000* vol. 3 314–317 vol.3 (IEEE, 2000).
29. Russakovsky, O. *et al.* ImageNet large scale visual recognition challenge. *Int. J. Comput. Vis.* **115**, 211–252 (2015).
30. Bottou, L. Stochastic Gradient Descent Tricks. in *Neural Networks: Tricks of the Trade: Second Edition* (eds. Montavon, G., Orr, G. B. & Müller, K.-R.) 421–436 (Springer Berlin Heidelberg, Berlin, Heidelberg, 2012).
31. Watkinson, A. R. & Zar, J. H. Biostatistical Analysis, 3rd edn. *J. Appl. Ecol.* **33**, 1230 (1996).
32. Ross, S. M. *Introduction to Probability Models.* (Academic Press, 2014).
33. Salvi, M., Acharya, U. R., Molinari, F. & Meiburger, K. M. The impact of pre- and post-image processing techniques on deep learning frameworks: A comprehensive review for digital pathology image analysis. *Comput. Biol. Med.* **128**, 104129 (2021).
34. Senaras, C., Niazi, M. K. K., Lozanski, G. & Gurcan, M. N. DeepFocus: Detection of out-of-focus regions in whole slide digital images using deep learning. *PLoS One* **13**, e0205387 (2018).
35. Rodrigues, D. *et al.* Abstract 5442: SlideQC: An AI-based tool for automated quality control of whole-slide digital pathology images. *Cancer Res.* **83**, 5442–5442 (2023).
36. Janowczyk, A., Zuo, R., Gilmore, H., Feldman, M. & Madabhushi, A. HistoQC: An

Open-Source Quality Control Tool for Digital Pathology Slides. *JCO Clin Cancer Inform* **3**, 1–7 (2019).

## Supplementary materials

Deep Blur Multi-Model (DeepBlurMM) - a strategy to mitigate the impact of unsharp image areas in computational pathology



Table S1. Data split at each CV

| <b>CV Folds</b> | <b>Division of Training Sets into 5 Training and 5 Tuning Sets for Each Cross-Validation Fold</b> |   |
|-----------------|---|---|
| CV 1            | <b>Training set 1 (N = 741)</b><br>Grade 1 N=293<br>Grade 3 N=448                                 | <b>Training set 1 (N = 592)</b><br>Grade 1 N = 234<br>Grade 3 N = 358 |
|                 |   | <b>Tuning set 1 (N = 149)</b><br>Grade 1 N = 59<br>Grade 3 N = 90     |
|                 | <b>Validation set1 (N = 175)</b><br>Grade 1 N = 70<br>Grade 3 N = 105                             |   |
| CV 2            | <b>Training set 2 (N = 742)</b><br>Grade 1 N = 295<br>Grade 3 N = 447                             | <b>Training set 2 (N = 592)</b><br>Grade 1 N = 236<br>Grade 3 N = 357 |
|                 |   | <b>Tuning set 2 (N = 149)</b><br>Grade 1 N = 59<br>Grade 3 N = 90     |
|                 | <b>Validation set 2 (N=174)</b><br>Grade 1 N = 68<br>Grade 3 N = 106                              |   |
| CV 3            | <b>Training set 3 (N = 748)</b><br>Grade 1 N = 296<br>Grade 3 N = 452                             | <b>Training set 3 (N = 598)</b><br>Grade 1 N = 237<br>Grade 3 N = 361 |
|                 |   | <b>Tuning set 3 (N = 150)</b><br>Grade 1 N = 59<br>Grade 3 N = 90     |
|                 | <b>Validation set 3 (N=168)</b><br>Grade 1 N = 67<br>Grade 3 N = 101                              |   |
| CV 4            | <b>Training set 4 (N = 728)</b><br>Grade 1 N = 285<br>Grade 3 N = 443                             | <b>Training set 4 (N = 582)</b><br>Grade 1 N = 228<br>Grade 3 N = 354 |
|                 |   | <b>Tuning set 4 (N = 146)</b><br>Grade 1 N = 57<br>Grade 3 N = 89     |
|                 | <b>Validation set 4 (N = 188)</b><br>Grade 1 N = 78<br>Grade 3 N = 110                            |   |
| CV 5            | <b>Training set 5 (N = 705)</b><br>Grade 1 N = 283<br>Grade 3 N = 422                             | <b>Training set 5 (N = 564)</b><br>Grade 1 N = 226<br>Grade 3 N = 338 |
|                 |   | <b>Tuning set 5 (N = 141)</b><br>Grade 1 N = 57<br>Grade 3 N = 84     |
|                 | <b>Validation set 5 (N = 211)</b><br>Grade 1 N = 80<br>Grade 3 N = 131                            |   |

Table S2. AUC Scores for three models

| Slide Level          |            |           |           | Tile Level           |            |           |           |
|----------------------|------------|-----------|-----------|----------------------|------------|-----------|-----------|
|                      | Model_base | Model_0.5 | Model_1.0 |                      | Model_base | Model_0.5 | Model_1.0 |
| <b>Original Set</b>  | 0.888      | 0.878     | 0.778     | <b>Original Set</b>  | 0.819      | 0.818     | 0.722     |
| <b>Blur set 0.5</b>  | 0.889      | 0.874     | 0.791     | <b>Blur set 0.5</b>  | 0.815      | 0.811     | 0.733     |
| <b>Blur set 1.0</b>  | 0.870      | 0.873     | 0.802     | <b>Blur set 1.0</b>  | 0.797      | 0.799     | 0.747     |
| <b>Blur set 1.5</b>  | 0.833      | 0.845     | 0.797     | <b>Blur set 1.5</b>  | 0.772      | 0.779     | 0.746     |
| <b>Blur set 2.0</b>  | 0.786      | 0.805     | 0.781     | <b>Blur set 2.0</b>  | 0.744      | 0.749     | 0.733     |
| <b>Blur set 2.5</b>  | 0.747      | 0.778     | 0.764     | <b>Blur set 2.5</b>  | 0.706      | 0.721     | 0.712     |
| <b>Blur set 3.0</b>  | 0.721      | 0.763     | 0.755     | <b>Blur set 3.0</b>  | 0.678      | 0.698     | 0.692     |
| <b>Blur set 3.5</b>  | 0.694      | 0.740     | 0.733     | <b>Blur set 3.5</b>  | 0.651      | 0.676     | 0.662     |
| <b>Blur set 4.0</b>  | 0.668      | 0.723     | 0.696     | <b>Blur set 4.0</b>  | 0.626      | 0.657     | 0.628     |
| <b>Blur set 5.0</b>  | 0.612      | 0.671     | 0.648     | <b>Blur set 5.0</b>  | 0.579      | 0.616     | 0.595     |
| <b>Blur set 6.0</b>  | 0.534      | 0.578     | 0.615     | <b>Blur set 6.0</b>  | 0.530      | 0.553     | 0.581     |
| <b>Blur set 7.0</b>  | 0.478      | 0.524     | 0.565     | <b>Blur set 7.0</b>  | 0.488      | 0.513     | 0.546     |
| <b>Blur set 8.0</b>  | 0.436      | 0.506     | 0.493     | <b>Blur set 8.0</b>  | 0.453      | 0.497     | 0.511     |
| <b>Blur set 9.0</b>  | 0.390      | 0.482     | 0.426     | <b>Blur set 9.0</b>  | 0.429      | 0.479     | 0.480     |
| <b>Blur set 10.0</b> | 0.395      | 0.465     | 0.406     | <b>Blur set 10.0</b> | 0.433      | 0.468     | 0.468     |